Results in Engineering 29 (2026) 108793

Contents lists available at ScienceDirect

Results in Engineering

journal homepage: www.sciencedirect.com/journal/results-in-engineering

Geometry and performance modelling of internally geared screw machines with comparison to conventional twin screw compressor ⋆

Halil Lacevic *, Ahmed Kovacevic, Sham Rane, Matthew Read

Centre for Compressor Technology, City St George's University, Northampton Square, EC1V 0HB, London, United Kingdom

ARTICLE INFO

Keywords:
Internally geared screw machine
Chamber model
Screw compressor

ABSTRACT

Internally geared screw machines (IGSMs) are a class of positive displacement compressors introduced in recent years. Their design involves two intermeshing rotors, denoted as the main (inner) and gate (outer), which rotate in the same direction on parallel but offset axes. Unlike conventional twin screw machines, which implement two externally geared rotors positioned side by side, IGSMs feature internal gearing, with one rotor enclosed within the other. While conventional twin screw compressors are widely used and extensively studied, IGSMs remain relatively novel. Previous research has primarily focused on their geometric feasibility and potential advantages using simplified performance models. This paper contributes by presenting a detailed geometrical model of an internally geared screw machine, enabling the calculation of geometry relevant parameters and integration with a well-established one-dimensional chamber model for performance prediction. The chamber model is compared to Computational Fluid Dynamics (CFD) for a single IGSM design operating under both oil-free and oil-injected conditions. Furthermore, the IGSM design is compared with a conventional twin screw configuration to provide a preliminary assessment of relative performance for a small-scale air compression application. The results are analysed, and directions for future work are outlined to support continued development and validation of this novel machine concept.

1. Introduction

Positive displacement machines are a type of mechanical devices that compress or move fluid (either gas or liquid) by trapping a fixed volume of fluid in a chamber and mechanically forcing it through the system. This process is achieved either by reducing the chamber volume or by displacing the fluid through the motion of mechanical components [1].

There are various types of positive displacement machines, typically classified based on their working principles. One widely used class is the twin screw compressor, which consists of two intermeshing helical rotors (referred to as the main and gate rotors) enclosed within a fixed casing. The main rotor is typically directly driven by an external motor, while the gate rotor is either driven through timing gears or by rotor contact, depending on the application type [2].

As the rotors rotate in opposite directions on parallel but offset axes, a series of enclosed working chambers is formed between the rotor lobes and the casing walls. During operation, low-pressure gas is drawn into working chambers through the intake port as the volume created between the meshing rotor surfaces increases. As rotation continues, the trapped volume of gas is progressively reduced due to the decreasing chamber volume. The compressed gas is then exposed to the discharge port once the chamber reaches the end of the compression process, and is pushed out of the machine as the volume reduces to zero.

This continuous process of gas intake, compression, and discharge occurs along the axial length of the rotors, providing a smooth and steady flow of compressed gas with high efficiency and reliability [3].

Twin screw compressor applications can be categorised into oil-free and oil-injected designs. In oil-free compressors, external timing gears are used to synchronise rotor rotation and reduce contact forces, as there is no oil to provide lubrication (although, in some cases, water injection may be used as an alternative for lubrication and cooling purposes [4]). Oil-free twin screw machines are commonly used in air compression applications requiring clean uncontaminated air, such as pharmaceutical manufacturing and food processing [5].

In contrast, oil-injected compressors introduce oil directly into the compression chamber through the oil injection port. By defining the position and size of the oil injection port, the amount of oil in the working chamber can be controlled. The oil serves multiple purposes in twin

⋆ This document is the results of the research project funded by Carrier Global Corporation, USA and PDM Analysis Ltd, UK.
* Corresponding author.
E-mail address: halil.lacevic@city.ac.uk, halil.lacevic@citystgeorges.ac.uk (H. Lacevic).
URL: https://www.lacevic.com (H. Lacevic)

https://doi.org/10.1016/j.rineng.2025.108793
Received 1 October 2025; Received in revised form 25 November 2025; Accepted 16 December 2025
Available online 19 December 2025

Nomenclature

N_1	Number of lobes on main rotor
N_2	Number of lobes on gate rotor
E	Axis distance between rotor centres
r_1	Main rotor pitch circle radius
r_2	Gate rotor pitch circle radius
L	Rotor length
D_1	Main rotor outer diameter
D_2	Gate rotor outer diameter
φ_1	Main rotor rotational angle
φ_2	Gate rotor rotational angle
Φ	Main rotor wrap angle
λ	Non-dimensional profile shape parameter
$\bar{\sigma}$	Non-dimensional profile shape parameter
θ	Profile parameter
ω_1	Main rotor rotational speed
P_1	Intake pressure
P_2	Outlet pressure

screw machines: it lubricates the rotors, seals internal clearances to reduce leakage, and removes heat generated during compression [6]. In such designs, the gate rotor is typically driven by direct contact with the main rotor, eliminating the need for timing gears. Oil-injected screw compressors are widely used in general industrial applications, such as automotive plants, pneumatic systems, and refrigeration [6].

Another class of positive displacement machines is the gerotor pump, commonly used in oil pumping applications such as lubrication systems and hydraulic motors [7,8]. Inspired by the internal meshing concept of gerotor designs, the internally geared screw machine (IGSM) was proposed several years ago as a novel variant of twin screw compressors [9,10]. Unlike conventional twin screw machines, which consist of two externally geared rotors positioned side by side, IGSMs feature an inner (main) rotor and an outer (gate) rotor with one additional lobe, where the outer rotor surrounds the inner rotor and meshes internally with it. Furthermore, the rotors rotate in the same direction on parallel but offset axes.

IGSMs operate on the same fundamental working principles as conventional twin screw machines, relying on the continuous intake, compression, and discharge in the working chambers. However, the key differences is the rotor configuration, which in IGSM features internal rather than external meshing, and in the location of the working chambers, which in IGSMs are formed between the lobes of the inner and outer rotors. Additionally, intake and discharge ports in IGSMs can only be arranged axially, in contrast to the radial port configuration possible in conventional designs [9].

Internally geared screw machines offer several potential advantages over conventional twin screw compressors, particularly in compact and small-scale applications. One of the potential benefits is the reduction of internal leakage due to the fully enclosed rotor configuration and the potential for tighter sealing along the internal meshing surfaces [9]. A further advantage is the absence of a blowhole area, since the internal meshing and axial porting of IGSMs allow the design to eliminate the need for a blowhole, thereby possibly improving efficiency [9].

To simulate and predict performance of conventional twin screw machines, various modelling approaches have been developed. These include both low-order models, such as the widely used one-dimensional chamber model [3], and high-order models based on Computational Fluid Dynamics (CFD) [11]. The chamber model offers a simplified but efficient means of simulating the pressure, temperature, and mass flow within the working chambers, incorporating empirical or analytical leakage correlations to estimate internal losses. In contrast, CFD provides a high-fidelity representation of the internal flow. These modelling tools are well established and have been extensively validated in the literature, forming the basis for design optimisation, performance evaluation, and operational diagnostics of conventional twin screw machines [12–14].

As IGSMs represent a relatively novel type of twin screw machine, prior research has primarily focused on rotor profiling methods [15] and the geometric characterisation of these machines [16], particularly the influence of different rotor shapes on overall geometry. While the geometric aspects have been well explored, only a limited number of studies have attempted to apply simplified non-validated one-dimensional performance prediction models [10,17] or Computational Fluid Dynamics (CFD) [18] to evaluate the potential benefits of the internally geared configuration.

This paper contributes by introducing a detailed geometry model in combination with an existing one-dimensional multi-chamber model applied to internally geared screw machines. The chamber model is compared against a high-fidelity CFD simulation for a representative design. These models are demonstrated through a dedicated case study of an internally geared screw machine. Furthermore, this paper presents, for the first time, an initial performance comparison between an IGSM and a conventional twin screw compressor in an oil-injected small-scale air compression application.

2. Modelling of internally geared screw machine

The production of twin screw compressors is both time-consuming and expensive, making it essential to develop robust and accurate digital models that can reliably simulate machine performance prior to manufacturing. Such models not only enhance understanding of the overall geometry and internal processes but also enable effective design optimisation.

Therefore, this section describes the principles used to develop a geometry model to enable the calculation of the key geometrical parameters of internally geared screw machines. A comprehensive geometry model of IGSMs requires the implementation of a rotor profiling method, evaluation of meshing conditions, calculation of working chamber volumes, leakage paths, and end port geometry.

Since IGSM design is derived from gerotor pumps, fundamental rotor profiling methods are based on the ones used for gerotor and progressive cavity pumps, where rotor profiles are predominantly defined using epitrochoidal curves [19,20].

Both gerotor pumps and IGSM rotor profiles must ensure continuous meshing between the rotors to maintain sealing of the working chambers. However, a key distinction lies in an additional geometric constraint specific to IGSMs, where the initial working chamber area must reduce to zero at the chamber formation to ensure proper sealing and compression behaviour.

In this paper the pin-generation rotor profiling method is adopted, originally introduced for gerotor mechanisms by Vecchiato et al. [20], and later applied to internally geared screw machines by Read et al. [16].

To ensure continuous rotor meshing, the Fundamental Law of Gearing must be satisfied. Also known as the meshing condition, this principle states that for a pair of rotors to maintain a constant velocity ratio, the normal at the point of contact between their profiles must always intersect a fixed point on the line connecting their centres, referred to as the pitch point [21]. The equations of the meshing conditions between the rotors are detailed by Vecchiato et al. [20] and are used in this work to determine locations of the contact points for each rotational position of the rotors.

The initial implementation of the pin-generation method for internally geared screw machines was introduced by Read et al. [16], using circular pins to generate rotor profiles. While various attempts have since been made to use elliptical, cosine, or other arbitrary curves as pin shapes to generate more complex or asymmetric rotor profiles [22–24], an analytical solution to the meshing condition exists only for the case

of circular pins. When arbitrary curves are used, the meshing condition must be solved numerically, increasing computational complexity.

To address this, Read et al. [25] also proposed a modified approach that maintains the analytical solvability of the meshing condition while still enabling the generation of asymmetric profiles by using a combination of circular pin segments, subject to certain geometric constraints. Although the introduction of asymmetric rotor profiles significantly improved the performance of conventional twin screw compressors, no clear performance benefit has yet been demonstrated for asymmetric designs in the context of internally geared screw machines.

Therefore, this paper focuses on symmetric rotor profiles generated using the pin-generation method with circular pins, ensuring analytical simplicity and satisfying the fundamental meshing condition. However, applying the same principles to asymmetric profiles is straightforward.

2.1. Rotor profiles

The shape of rotor profiles generated using circular pins is defined by two key non-dimensional parameters. The first, $\lambda = a/r_2$, defines the relative position of the circular pin, where a is the distance from the global coordinate origin to the centre of the pin, and r_2 denotes the pitch circle radius of the outer rotor.

The second parameter, $\sigma = \rho/r_2$, represents the ratio of the pin radius ρ to the outer rotor's pitch circle radius. Since certain values of σ can lead to undercuts in the resulting rotor profile, Read [16] introduced a modified, normalised parameter $\bar{\sigma} \in [0, 1]$, where the upper limit corresponds to the maximum allowable pin size $\sigma_{\max} = \sigma_{\lim}$. This reformulation allows $\bar{\sigma}$ to be interpreted as a percentage of the limiting value, ensuring that valid and manufacturable rotor profiles are generated for any choice of $\bar{\sigma}$ within the unit interval.

When generating rotor profiles using the pin-generation method, in addition to specifying the non-dimensional shape parameters λ and $\bar{\sigma}$, it is also necessary to define the number of lobes on either the main (inner) or gate (outer) rotor, typically number of lobes on the main rotor N_1, as number of lobes on the gate rotor $N_2 = N_1 + 1$ in many IGSM configurations. Furthermore, one of the key geometric dimensions, either the axis distance E or the maximum outer rotor diameter D, must be selected, since they are directly related through the geometric constraint given in Eq. (1).

$$\frac{E}{D} = \frac{1}{2N_2\left(\lambda - \sigma + \frac{2}{N_2}\right)} \tag{1}$$

These relationships define the geometric scaling required to ensure proper rotor meshing and profile construction within the IGSM framework. The geometric foundation and construction principles of the pin-generation method using circular pins are illustrated in Fig. 1. Fig. 2 shows examples of rotor profile shapes for $N_1 = 5$ and $N_2 = 6$, where N_1 and N_2 denote the number of lobes on the main (inner) and gate (outer) rotors, respectively. The influence of varying the parameters λ and $\bar{\sigma}$ on the resulting rotor geometries is also demonstrated.

2.2. Geometry

Once the rotor profiles are generated, the overall geometry of the machine can be computed. The pin-generation method requires the selection of non-dimensional rotor shape parameters along with either the axis distance or the outer rotor diameter, which fully constrains the rotors in two dimensions.

To evaluate the machine geometry in three dimensions, it is first necessary to define the rotor length L. Additionally, since the rotors are helical, the wrap angle Φ must also be specified. The wrap angle can be defined for one of the rotors, typically the main rotor, and calculated for the other using the gearing ratio. The relationship is given in Eq. (2), where Φ_1 and Φ_2 are the wrap angles of the main and gate rotors, respectively, and N_1 and N_2 are their corresponding lobe counts.

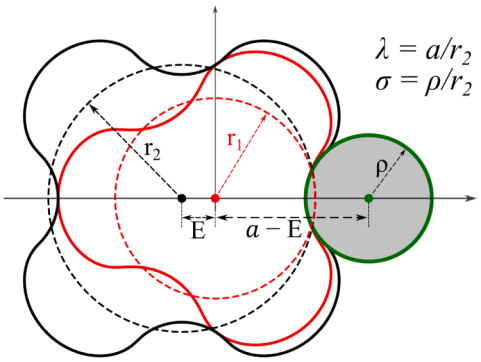

Fig. 1. Geometric construction and coordinate system used in the pin-generation method for internally geared screw machines. The diagram illustrates the positioning of the circular pin, the pitch circles of the inner and outer rotors, and key geometric parameters such as a, r_2, and ρ.

Table 1
Representative internally geared screw machine configuration adopted from prior CFD analysis of internally geared screw machines. Rane et al. [18].

Unit	Value	Description
(–)	6	Outer rotor lobe number (N_2)
(–)	5	Inner rotor lobe number (N_1)
(mm)	100	Diameter of outer rotor (D_2)
(mm)	130	Length of both rotors (L)
(mm)	6.712	Axis spacing distance (E)
(–)	1.4	Profile shape parameter (λ)
(–)	0.8	Profile shape parameter ($\bar{\sigma}$)
(°)	234	Inner rotor wrap angle (Φ_1)
(–)	2	Built-in volume ratio (VI)

$$\Phi = \Phi_1 = \frac{N_2}{N_1}\Phi_2 \tag{2}$$

A representative case study, summarised in Table 1 and based on the previous work by Rane et al. [18], is introduced to demonstrate the developed geometry model of the IGSM. This configuration is used throughout the paper to illustrate the procedures for calculating the IGSM geometry.

Initial step to calculate geometry of IGSM is the identification of the working chamber. To identify working chambers in a given rotor position it's important to determine sealing lines or locations of the contact points in the global coordinate system. When generating rotors using circular pins in pin generation method, consequently the meshing condition is solved where the solutions specify the locations of the contact points for each rotational position of the rotors.

To calculate the area of a single working chamber from its initial formation to the point where it disappears, the leading and trailing contact points are used to define its boundaries. At any given rotor position, the chamber is enclosed between these two contact points and the corresponding segments of the inner and outer rotor profiles.

The rotor profile coordinates are defined using the meshing condition, which relates the angular position of a point on the rotor lobe, θ, to the current rotational position of the rotor, φ. For the main and gate rotors, the profiles are expressed as $x_i(\theta, \varphi_i)$ and $y_i(\theta, \varphi_i)$, $i \in [1, 2]$, where θ is the profile parameter, and the rotational positions of the rotors are given by $\varphi_1 = \varphi$ and $\varphi_2 = \frac{N_1}{N_2}\varphi_1$, based on the lobe count ratio between the two rotors.

As described by Vecchiato et al. [20], the meshing condition includes the rotor rotational position φ as an input, and solving it gives the corresponding values of θ that determine the contact points between the

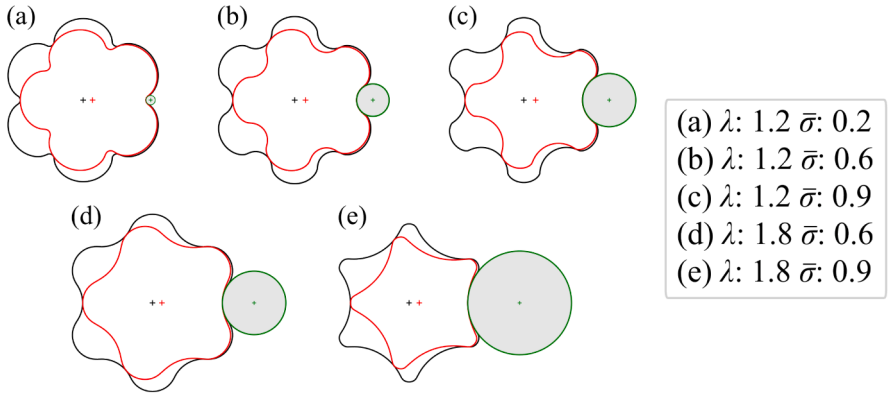

Fig. 2. Examples of rotor profile shapes for $N_1 = 5$ and $N_2 = 6$, showing the effect of varying the non-dimensional parameters λ and $\bar{\sigma}$. These parameters influence the shape and size of the working chambers, as well as the sealing characteristics of the rotor pair.

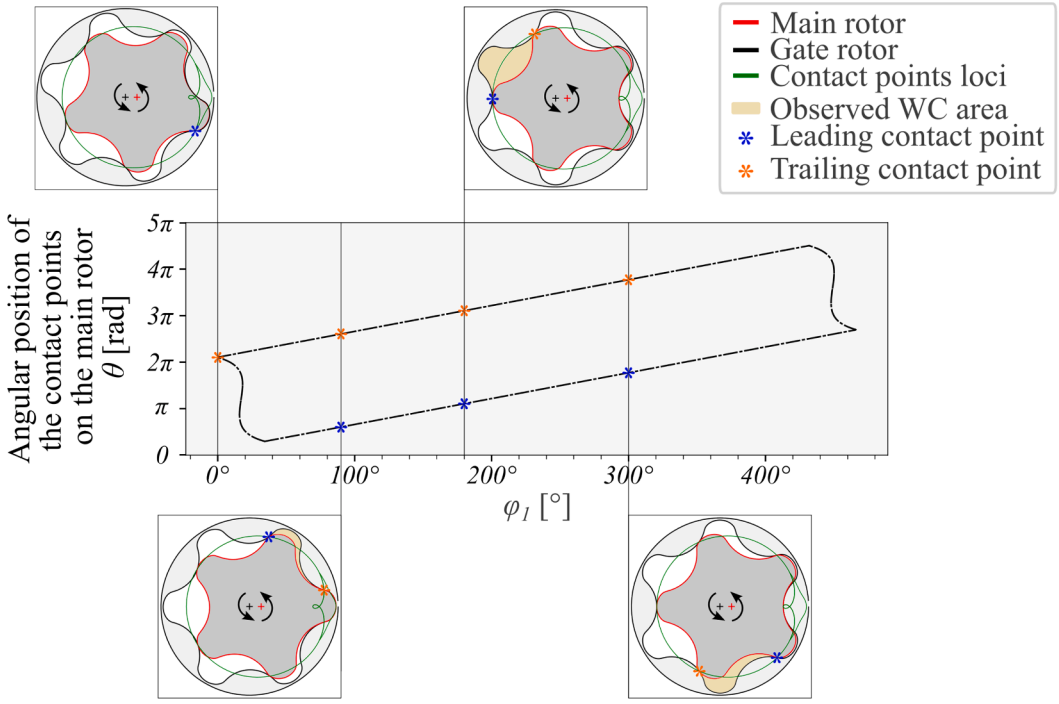

Fig. 3. Tracking of the leading and trailing contact points for a single working chamber over one rotation cycle of the main rotor. The tracked working chamber is illustrated for four selected angles, showing the chamber formation, growth, and closure.

rotors. These angular values identify which points on the rotor profiles are in contact for a given rotor position.

For each rotor rotational position φ, the meshing condition is solved to obtain the corresponding angular positions θ of the contact points on the main and gate rotors. Using these values, the contact point coordinates $x_i(\theta)$, $y_i(\theta)$ are computed in the local, non-rotated frame of each rotor. To obtain the positions of the contact points in the actual physical configuration, these coordinates are then rotated about the respective rotor origins by the current rotor angles, φ_1 and φ_2.

An example of the relationship between the main rotor's rotational position, φ_1, and the meshing condition solutions, θ, for the representative case given in Table 1, is shown in Fig. 3. At the initial position, $\varphi_1 = 0$, both the leading and trailing contact points coincide, resulting in a working chamber area of zero. Three additional positions are also shown, illustrating how the chamber evolves and can be tracked throughout the rotation.

This procedure enables the identification of working chamber boundaries at each rotor position, which is essential for accurate calculation of IGSM geometry throughout the operating cycle.

Once the working chamber has been identified, its cross-sectional area must be calculated at each rotor position to understand how it evolves over a full rotation. This corresponds to evaluating the two-dimensional cross-section of the rotors at successive rotational positions. In three dimensions, this results in a volume bounded along the axial direction, where the working chamber grows from zero, reaches a maximum, and then returns to zero as it progresses along the machine's length.

Various numerical approaches can be used to calculate the chamber area for a given position. In this paper, an efficient method based on precomputed cumulative rotor areas is implemented. The total area enclosed by each rotor is first evaluated for a reference position (initial position of the rotors). Then, once the leading and trailing contact points are determined for any given rotor angle, the partial rotor areas bounded between these two points can be extracted from the cumulative data. To improve accuracy, a triangular correction, formed by connecting the contact points with the respective rotor origins, is applied to each rotor segment. The working chamber area is finally obtained by subtracting the corrected inner rotor segment area from the corresponding outer rotor segment area.

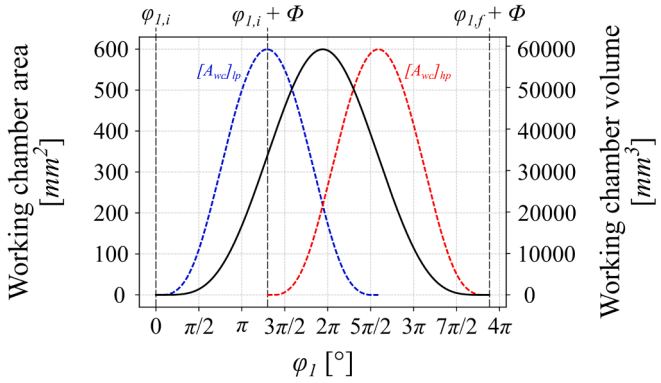

Fig. 4. Evolution of the working chamber area and volume over the main rotor angle φ_1. The low-pressure and high-pressure side areas $[A_{wd}]_{lp}$ and $[A_{wd}]_{hp}$ are shown in blue and red, respectively, with the total working chamber volume illustrated in black. (For interpretation of the references to colour in this figure legend, the reader is referred to the web version of this article.)

To determine the volume of a working chamber at a given main rotor angle $\varphi_{1,g}$, the corresponding two-dimensional cross-sectional area must be integrated along the axial length of the rotor. This reflects how the chamber extends helically from the low-pressure to the high-pressure end face of the machine.

Let $A_{\mathrm{wc}}(\varphi_1, z)$ denote the working chamber area at rotor angle φ_1 and axial position z. The total chamber volume can be obtained by integrating this area over the full rotor length L. However, due to the helical nature of the rotors, this three-dimensional integration can be reformulated in terms of the angular progression of the rotor using the wrap angle Φ_1, which defines the total angular span over which the chamber evolves. As shown by Read et al. [16], the resulting expression is given by:

$$V_{\mathrm{wc}}(\varphi_{1,g}) = \int_0^L A_{\mathrm{wc}}(\varphi_1, z)\, dz = \frac{L}{\Phi_1} \int_{\varphi_{1,i}}^{\varphi_{1,g}} \left([A_{\mathrm{wc}}]_{\mathrm{lp}} - [A_{\mathrm{wc}}]_{\mathrm{hp}}\right) d\varphi_1$$

Here, $\varphi_{1,i}$ denotes the angular position where the chamber first begins to form, and $\varphi_{1,g}$ is the current rotor angle for which the volume is evaluated. The terms $[A_{\mathrm{wc}}]_{\mathrm{lp}}$ and $[A_{\mathrm{wc}}]_{\mathrm{hp}}$ represent the cross-sectional chamber areas at the low-pressure and high-pressure end faces, respectively. The scaling factor $\frac{L}{\Phi_1}$ maps the angular rotation into axial displacement, allowing the chamber volume to be computed based only on cross-sectional area data at each end face. This approach provides an efficient and accurate method to compute the evolving chamber volume as the rotors rotate, as required for performance modelling. An example of volume calculation for the representative case from Table 1 is shown in Fig. 4.

Once the full chamber volume has been calculated over the entire chamber evolution cycle, the swept volume V_{sw}, defined as the theoretical volume displaced per revolution of the main rotor, can be obtained using Eq. (3).

$$V_{sw} = N_1 \max(V_{\mathrm{wc}}) \tag{3}$$

Due to the nature of the compression process in internally geared screw machine, the working chambers operate at varying pressure levels along the rotor length. As a result, leakage can occur through small internal clearances between moving and stationary components, allowing high-pressure gas to escape into lower-pressure regions. These leakages reduce the overall volumetric efficiency and performance of the machine.

Leakage paths in internally geared screw machines occur along specific sealing lines that connect neighbouring working chambers operating at different pressures. As illustrated in Fig. 5, each working chamber is bounded by sections of the rotor profiles, with contact lines that may interface either with a chamber ahead (higher pressure) or behind (lower pressure) along the rotor axis.

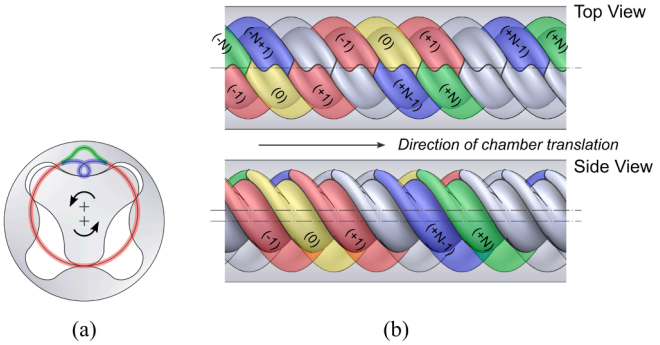

Fig. 5. Illustration of leakage paths in an internally geared screw machine (third-angle projection). (a) rotor rotation and chamber positions; (b) top and side views of chamber indexing along the axial direction. Leakage may occur between adjacent chambers as they translate during operation.

The sealing lines illustrated in Fig. 5 represent the primary leakage paths in the IGSM configuration. These include the main leakage path: from the outer rotor tip to the main rotor tip (red), the inner path: from the outer rotor tip to the inner rotor root (blue), and the outer path: from the outer rotor root to the inner rotor tip (green).

To calculate the leakage areas for a given chamber at a specific rotor position, the relevant contact points are identified in three dimensions. The segment length along each corresponding sealing line is then expressed as a function of the main rotor rotational position, $\mathcal{L}(\varphi_1)$, and the leakage area is evaluated using Eq. (4), where δ_ℓ denotes the predefined clearance gap size.

$$A_\ell = \delta_\ell \mathcal{L}(\varphi_1) \tag{4}$$

In internally geared screw machines, compression is achieved by the geometry of the end plates, which regulate the timing of fluid entry and exit through the ports [9]. Therefore, a critical step in performance prediction is the accurate estimation of port opening areas as a function of rotor rotational position. In this study, the port shapes are determined numerically in the polar coordinate system, using geometric boundaries such as rotor profiles, contact loci, and bounding circles.

To construct the inlet port shape, the rotor position at which the working chamber reaches its maximum volume is first identified. At this position, two bounding regions are defined in the polar coordinate system:

- The outer boundary is defined by the gate rotor tip circle, the main rotor root circle and contact loci (Fig. 6 (a) Polygon I).
- The inner region, defined as Polygon II (Fig. 6 (a)), follows the segments of the rotor profiles and the contact loci bounded between the trailing and leading contact points.

The final inlet port shape is determined by clipping Polygon I with Polygon II, resulting in the blue shaded region shown in Fig. 6 (a). This clipped polygon is then transformed from the polar coordinate system to the physical domain to obtain the final port shape, also illustrated in Fig. 6 (a).

The same geometric principles apply to the construction of the discharge port. However, instead of maximum chamber volume, the relevant reference point is defined by the volume index VI, which specifies the relative rotational position at which the working chamber should begin to discharge. For the representative configuration described in Table 1, a value of $VI = 2$ is used, and the corresponding discharge port formation is illustrated in Fig. 6 (b). As with the inlet, two polygons are defined to compute the discharge port shape:

- Polygon I (Fig. 6 (b)) is defined by the gate rotor tip circle, the main rotor root circle, the relevant segments of the rotor profiles, and the contact loci associated with the working chamber identified by the selected volume index.

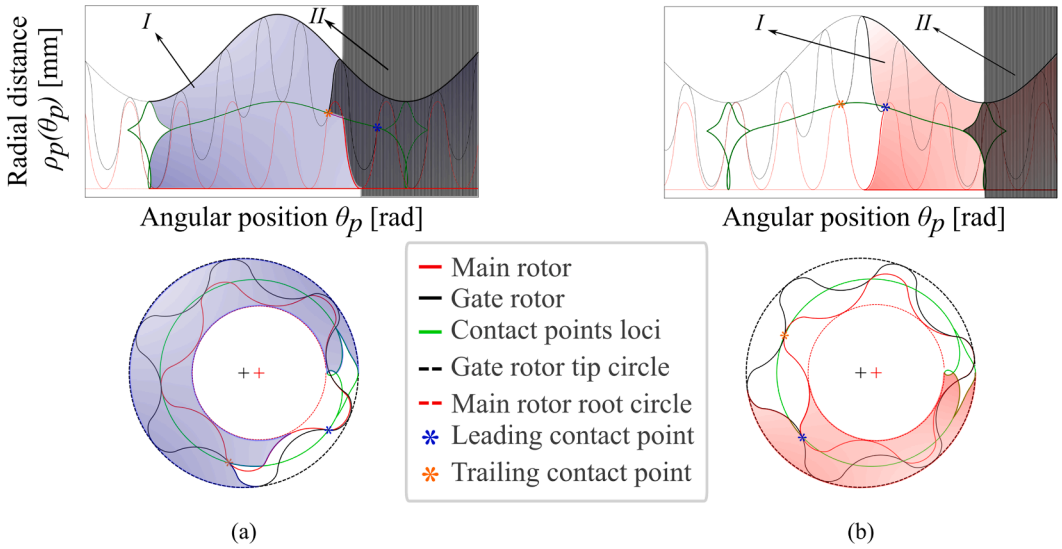

Fig. 6. End port formation process for the internally geared screw machine. Top plots show the key curve sections for port definition in polar coordinate system. Bottom views illustrate the corresponding shaded regions that define the final end port geometry for the inner (a) and outer (b) rotors. Leading and trailing contact points determine the angular boundaries of the port openings.

- Polygon II (Fig. 6 (b)) is based on the contact loci.

The final discharge port shape is determined by clipping Polygon I with Polygon II, resulting in the red shaded region shown in Fig. 6 (b). The final discharge port shape in physical domain is also illustrated.

Port flow areas relative to the main rotor's rotational position can be determined numerically by constructing a polygon for the tracked working chamber at each rotational step and calculating its intersection with the corresponding port shape polygon. While the resulting port geometries display sharp features that may present manufacturing challenges, they represent theoretical maximum openings. As these features occur when the chamber area is small, they can likely be smoothed in practice without significantly affecting performance, however, this aspect is beyond the scope of the present study.

2.3. Chamber model

Simulation tools for conventional twin screw machines are well established and have been widely applied in past research. One such tool, SCORG, was developed at City, St George's, University of London and includes an implementation of the one-dimensional chamber model for performance prediction [11]. While this chamber model has been extensively used and validated for conventional twin screw machines [26–28], its application to internally geared screw machines has not been thoroughly investigated. Although the fundamental modelling principles remain the same, the distinct geometric configuration of IGSMs requires additional analysis to ensure the reliability and accuracy of chamber model predictions.

The implemented chamber model solves the unsteady internal energy conservation equation, enabling the calculation of thermodynamic and fluid properties within the machine over multiple cycles until convergence is achieved [3]. This process is governed by Eq. (5), which accounts for the energy gain due to gas inflow, denoted as $(\dot{m}h)_{\text{in}}$, and the energy loss resulting from gas outflow, given by $(\dot{m}h)_{\text{out}}$, where $\dot{m}$ is the mass flow rate and h is the specific enthalpy of the fluid. The internal energy of the gas is denoted by U, and $\dot{Q}$ represents the heat transfer between the working fluid and the compressor surroundings. Instantaneous pressure within the control volume is denoted by p, while the rate of change of volume with respect to the rotor's rotational position is expressed as $\frac{dV}{d\varphi_1}$. The angular velocity and angular position of the main rotor are denoted by ω_1 and φ_1, respectively.

$$\omega_1 \frac{dU}{d\varphi_1} = (\dot{m}h)_{in} - (\dot{m}h)_{out} + \dot{Q} - \omega_1 p \frac{dV}{d\varphi_1} \tag{5}$$

The mass continuity equation used in the chamber model is given by Eq. (6), which expresses the rate of change of mass within the control volume. Both the inflow mass rate, $\dot{m}_{\text{in}}$, and the outflow mass rate, $\dot{m}_{\text{out}}$ are defined using Eq. (7), where w is the fluid velocity, ρ is the instantaneous fluid density, and A is the corresponding flow cross-sectional area. The instantaneous density ρ is computed as the ratio of mass m to control volume V.

$$\omega_1 \frac{dm}{d\varphi_1} = \dot{m}_{\text{in}} - \dot{m}_{\text{out}} \tag{6}$$

$$\dot{m} = w\rho A \tag{7}$$

By solving the energy and continuity equations simultaneously, the model yields the variation of internal energy $U(\varphi_1)$ and mass $m(\varphi_1)$ over the rotor angle. Alongside the known chamber volume $V(\varphi_1)$, this allows for the calculation of specific internal energy $u = \frac{U}{m}$ and specific volume $v = \frac{V}{m}$. Assuming an ideal gas, the corresponding temperature T and pressure p inside the working chamber can be obtained using Eq. (8), where γ is the adiabatic exponent and R is the gas constant. Both γ and R, as well as the values of u and v, are known or determined from the model.

$$T = (\gamma - 1)\frac{u}{R}, \qquad p = \frac{RT}{v} \tag{8}$$

Clearance leakage mass flow rate, denoted by $\dot{m}_l$, is expressed in terms of local variables along the leakage path using Eq. (7). Leakage paths are assumed to have a rectangular cross-section with sealing line length L and clearance δ. The leakage velocity w_l is obtained from the differential momentum equation (Eq. (9)), which accounts for wall friction f as a function of the local Reynolds number, Mach number and clearance gap geometry. In this formulation, dx denotes the differential path length and D_e is the equivalent hydraulic diameter.

$$w_l, dw_l + \frac{dp}{\rho} + f\frac{w_l^2}{2}\frac{dx}{D_e} = 0. \tag{9}$$

Assuming an isothermal throttling process, the temperature variation of the working fluid across the leakage path is small, so the density may be treated as a function of pressure only. Under this assumption,

the governing equations can be integrated over the pressure drop between the high and low pressure sides, yielding the leakage mass flow rate given in Eq. (10), where p_2 and p_1 are the high and low side pressures, a is the speed of sound, and ζ is a dimensionless flow-resistance parameter.

$$\dot{m}_l = A_l \rho_l w_l = A_l \sqrt{\frac{\gamma\left(p_2^2 - p_1^2\right)}{a^2\left[\zeta + 2\ln\left(p_2/p_1\right)\right]}}. \tag{10}$$

For machines with liquid injection, the effective clearance gap is reduced by the instantaneous volume ratio of gas to the gas-liquid mixture in the working chamber. If only gas is present, this ratio is equal to 1, whereas it approaches 0 when the chamber is completely filled with liquid. During operation, it can take any value between these two limits.

The thermodynamic process within the compressor is described in detail by Hanjalic and Stosic [3], and the model used in this study is based on their formulation. The detailed chamber model will be verified by comparison with computational fluid dynamics (CFD) results for a representative case selected from Table 1.

2.4. Computational fluid dynamics

The main purpose of the CFD model in this study was to be able to verify the implementation of the IGSM geometry and thermodynamics calculation algorithms. CFD modelling for design and verification is common in twin screw compressors and pumps and literature provides example where performance of the machine is validated using test data [4–6,11]. Recently, these modelling principles were applied by the authors to firstly develop a CFD computational grid for IGSM and perform design calculation on an oil injected compressor for prototype study in [18]. The deforming rotor grid generation for IGSM is fully parametric and has been implemented in the customised grid generator SCORG [11]. The geometry and helical shape of the rotor was verified with CAD models.

Previous studies using the same CFD modelling methodology have shown that variations in integral quantities such as volumetric and adiabatic efficiency with grid density and time step size remain within 2-10 % and are therefore not significant for validation purposes [29]. In the present work, the quantities of interest are the cyclic integrals of mass flow rate and rotor torque, and the clearance gap size is predefined in the deforming mesh. In addition, the time step size is directly determined from the deforming mesh transition in degrees per step and the operating rotational speed of the inner rotor, which yields a fixed time step for each rotational speed. For these reasons, additional grid and time step independence studies have not been performed.

All wall boundaries in the CFD model are treated as adiabatic. The simulations use a pressure-based coupled transient solver with 20 iterations per time step, and a relaxation factor of 0.5 is applied to maintain stability over the pressure cycles.

This prototype IGSM was evaluated with an oil injection located on the high-pressure end plate with the injection timed to begin at 30 degrees past the suction port closure. Main parts of the CFD model are the rotors (volume deforms with time during the simulation), suction, discharge, and oil injection ports. Additionally, the operating clearances were specified as 100 μm between the rotors, the axial clearance at suction side was set to 100 μm and that at the discharge end was set at 50 μm. Oil injection diameter was 5 mm and the injection pressure was set equal to the discharge pressure. The description of the dry air CFD model for screw compressors [5] and two fluid CFD model suitable for oil injected compressors [6] has been used in [18] and in the current study. The same parameters for the ANSYS CFX solver, air and oil properties have been used. Mesh deformation is managed using a user defined function, all advection and transient schemes are set to second order accuracy. The SST k-Omega turbulence model is a common practise in these models and has been applied. At the Inlet and Oil injection a total pressure and temperature boundary condition is applied, while at the outlet a static pressure is applied. Flow of the air as well as oil is produced as a solution variable. Cyclically repetitive flow field is obtained after several time steps and data from the final compression cycles is used to estimate the average performance parameters such as mass flow rate (this quantifies leakage and volumetric efficiency), indicated power, specific power, discharge temperature, oil flow rate, and adiabatic efficiency. These data are then used to verify the chamber model predictions under similar operating conditions.

Table 2
Operating conditions used for comparison between CFD and chamber model for both oil-free and oil-injected IGSM configurations.

$\mathbf{P_1}$ [bar]	$\mathbf{P_2}$ [bar]	ω_1 [rpm]
Oil-Free		
1	2	2000
1	2	3000
1	2	4000
1	3	3000
1	3	4000
Oil-Injected		
1	2	2000
1	2	3000
1	2	4000
1	3	2000
1	3	3000
1	3	4000

3. Comparison of chamber model and CFD for IGSM

Developing reliable and accurate performance prediction models for internally geared screw machines is a crucial step in the design process. While CFD tools have become widely used in the analysis of positive displacement machines, they are often computationally intensive and time-consuming. As a result, there is significant value in implementing a robust and efficient chamber model capable of delivering faster simulations. Such models are particularly beneficial in optimisation studies, where a large number of simulations must be conducted to explore the design space and identify optimal configurations.

In this study, a one-dimensional chamber model has been integrated for IGSMs and its performance is evaluated. Although experimental validation is the most appropriate means of verifying such a model, the experimental test rig for IGSMs is currently under development with the numerical models providing insight to guide the design of a prototype machine. Therefore, to assess the chamber model's accuracy and to support understanding of its behaviour, a comparison is made with a higher-fidelity CFD model.

The CFD simulations used for this comparison are taken from previous work by Rane et al. [18], based on the representative machine configuration summarised in Table 1. Both models, chamber and CFD, are evaluated for oil-free and oil-injected conditions across a range of discharge pressures and rotor speeds. The cases included in this comparison are listed in Table 2.

Fig. 7 compares the predictions from the chamber model and CFD simulations for various performance parameters across a range of main rotor speeds and discharge pressures in oil-free operation. The corresponding numerical values of the CFD and chamber model predictions for these oil-free cases are summarised in Tables 3 and 4, respectively.

The chamber model accurately predicts the air flow rate (Fig. 7 (a)), showing excellent agreement with CFD results at both 2 bar and 3 bar discharge pressures. Although a slight mismatch is observed at lower rotor speeds, the linear trend with increasing speed is well captured.

Table 3
CFD model results for the oil-free IGSM configuration listed in Table 1, used for comparison with the chamber model in Fig. 7.

P_2 (bar)	ω_1 (rpm)	Q (m^3/min)	Power (W)	η_v (%)	T_2 (°C)	P_{sp} (kW/(m^3/min))	η_{ad} (%)
2	2000	0.16	820	27.64	240	5.01	25.50
2	3000	0.49	1274	55.76	158	2.57	49.70
2	4000	0.81	1735	68.56	132	2.14	59.80
3	3000	0.24	2265	26.72	420	9.55	22.50
3	4000	0.62	2952	52.51	268	4.75	45.30

Table 4
Chamber model results for the oil-free IGSM configuration listed in Table 1, used for comparison with the CFD results in Fig. 7.

P_2 (bar)	ω_1 (rpm)	Q (m^3/min)	Power (W)	η_v (%)	T_2 (°C)	P_{sp} (kW/(m^3/min))	η_{ad} (%)
2	2000	0.21	890	32.06	187	4.19	30.58
2	3000	0.51	1349	57.45	157	2.65	48.23
2	4000	0.81	1817	68.84	138	2.23	57.20
3	3000	0.24	2530	27.28	470	10.46	20.56
3	4000	0.61	3284	51.57	293	5.39	39.93

Table 5
CFD model results for the oil-injected IGSM configuration listed in Table 1, used for comparison with the chamber model in Fig. 8.

P_2 (bar)	ω_1 (rpm)	Q (m^3/min)	Power (W)	η_v (%)	T_2 (°C)	P_{sp} (kW/(m^3/min))	η_{ad} (%)
2	2000	0.35	774	58.98	72.50	2.22	57.50
2	3000	0.60	1228	67.83	81.50	2.04	62.60
2	4000	0.86	1740	72.94	101.50	2.02	63.30
3	2000	0.32	1278	54.14	71.60	3.99	53.80
3	3000	0.55	1995	61.81	83.40	3.64	59.10
3	4000	0.81	2764	68.39	94.40	3.42	62.90

Table 6
Chamber model results for the oil-injected IGSM configuration listed in Table 1, used for comparison with the CFD results in Fig. 8.

P_2 (bar)	ω_1 (rpm)	Q (m^3/min)	Power (W)	η_v (%)	T_2 (°C)	P_{sp} (kW/(m^3/min))	η_{ad} (%)
2	2000	0.32	799	54.04	66.73	2.50	51.08
2	3000	0.60	1246	67.82	74.04	2.07	61.63
2	4000	0.88	1734	74.74	79.41	1.96	65.09
3	2000	0.25	1331	43.19	77.46	5.22	41.24
3	3000	0.53	2011	60.21	88.99	3.77	57.08
3	4000	0.81	2723	68.72	97.37	3.35	64.16

Predicted input power shows good agreement (Fig. 7 (b)), especially at discharge pressure of 2 bar. For 3 bar, the chamber model slightly over-predicts the required power compared to CFD, but the trend with increasing speed remains consistent.

While the chamber model shows similar trends to CFD for specific power (Fig. 7 (c)), a larger deviation is observed at higher discharge pressures. Still, the model reasonably captures the decreasing trend of specific power with speed.

Volumetric efficiency is slightly overestimated by the chamber model (Fig. 7 (d)), particularly at lower pressure ratio. However, the model successfully follows the increasing efficiency trend with rotor speed, maintaining an acceptable level of accuracy.

Fig. 8 compares the performance predictions of the chamber model with CFD results for oil-injected operation of the internally geared screw machine. The comparison includes various performance parameters for the evaluated cases. The corresponding numerical values of the CFD and chamber model predictions for these oil-injected cases are summarised in Tables 5 and 6, respectively.

In Fig. 8 (a), the air flow rate predicted by the chamber model shows decent agreement with CFD across all operating conditions. Both models capture the linear increase in flow rate with rotor speed. This indicates the chamber model's robustness in simulating flow behaviour under oil-injected conditions.

Fig. 8 (b) presents the power input required by the machine. The chamber model closely tracks the CFD results for evaluated cases. The increasing trend is also captured accurately suggesting that the behaviour of chamber model is sufficient.

Fig. 8 (c) shows the specific power, a critical indicator of energy efficiency. The chamber model generally agrees with CFD trends, with specific power decreasing as speed increases. For lower speed, however, the chamber model tends to over-predict specific power.

Fig. 8 (d) illustrates the volumetric efficiency, defined as the ratio between simulated and theoretical volumes. The chamber model effectively captures the efficiency improvement with increasing rotor speed and aligns well with CFD predictions at higher speeds. However, a noticeable discrepancy is observed at the lowest speed, indicating reduced accuracy under these conditions.

Overall, the chamber model performs reliably for oil injected operation, reproducing key trends and magnitudes across performance metrics. Discrepancies between the CFD and chamber model are evident at low speeds and higher discharge pressures, which is expected given the complexity of flow modelling and heat transfer in oil injected machines that are not explicitly resolved in the chamber model, and such differences have also been reported for conventional twin screw machines in the literature [30]. A more detailed investigation of these discrepancies will be carried out once full experimental validation data becomes available. Nevertheless, since the primary focus of the present study is on higher speeds, where good agreement is observed, the use of the chamber model in the current analysis is considered appropriate and these results support its suitability for design exploration and optimisation tasks where rapid performance estimation is required.

4. Comparison of IGSM with conventional twin screw machine

A reliable chamber model for internally geared screw machines enables performance prediction and supports meaningful comparisons with established configurations in conventional twin screw compressors. Among the predicted advantages of IGSMs is their potential to extend the lower operating range of screw compressors, offering a promising alternative to scroll machines in small-capacity applications.

This section presents, for the first time, a performance comparison between an IGSM and the well-known and validated V60 compressor, a representative of one of the smallest commercially available conventional twin screw machine [31]. The V60 features a main rotor diameter of 59.7 mm and a 4/5 rotor lobe configuration. For a fair comparison, the IGSM45 is designed with the same rotor configuration (4/5), matched main rotor outer diameter, and equivalent displacement volume (approximately 0.150 l/rev). The IGSM45 rotor profiles are generated using the pin-generation method, adopting the same non-dimensional shape parameters λ and $\bar{\sigma}$ as in the configuration reported in previous work by Rane et al. [18], which was also used to compare the chamber model and CFD in Section 3 (see Table 1).

Both machines operate with air as the working fluid and are evaluated under oil-injected conditions. Oil is injected at 40°C through a 6 mm injection port at an angle of 60°. Performance is assessed across a range of main rotor tip speeds from 20 to 40m/s and pressure ratios $P_d \in [7, 10, 13]$. The volume index is set to $V_i = 4$ for both designs.

A summary of key geometric parameters for the IGSM45 and V60 is provided in Table 7, and the corresponding rotor profiles are illustrated in Fig. 9. From Table 7, it can be noticed that, for a matched main rotor outer diameter, the IGSM rotors must be longer to achieve the same displacement volume as the conventional twin screw machine.

To ensure a fair comparison, the clearance gaps in IGSM45 are matched to those of the V60. As blow-hole leakage is absent in internally geared screw machines, only radial and axial clearances are considered.

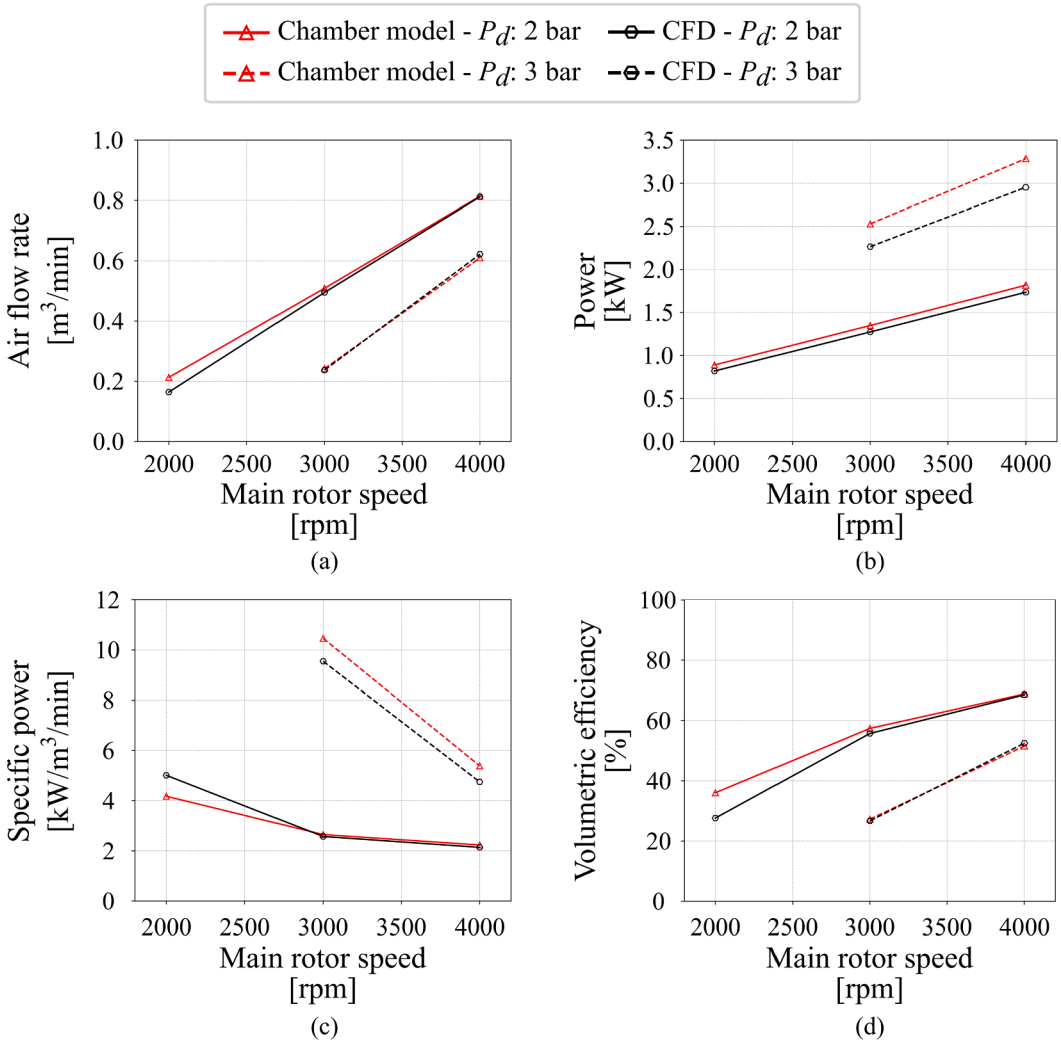

Fig. 7. Comparison between the chamber model and CFD results for the oil-free internally geared screw machine configuration specified in Table 1, evaluated for operating conditions defined in Table 2. The plots show: (a) air flow rate, (b) indicated power, (c) specific power, and (d) volumetric efficiency, across varying main rotor speeds for two pressure ratios.

Table 7
Geometry parameters of the compared V60 and IGSM45 compressors.

Parameter	IGSM45	V60
N_1	4	4
N_2	5	5
A	6.92 mm	42 mm
D_1	59.712 mm	59.695 mm
D_2	71.132 mm	47.308 mm
L	136.32 mm	92.528 mm
Φ_1	300°	300°
Displacement	0.150 l/rev	0.150 l/rev
VI	4	4

The V60 clearances are first tuned to reproduce the performance predictions reported in the technical catalogue [31]. Subsequently, for IGSM45 both the radial and axial clearance gaps are set equal to those of the V60 at 15 μm, while the V60 interlobe clearance, which corresponds to the inner and outer leakage paths in the IGSM (defined in Section 2.2), is also matched and set to 10 μm.

Fig. 10 (a) presents the predicted air flow rates for both the IGSM45 (solid lines) and compared V60 (dashed lines) machines over a range of main rotor speeds and discharge pressures. As expected, the flow rate increases linearly with rotor speed for all cases.

Fig. 10(b) compares the shaft power consumption against the flow rate for both IGSM45 and V60 compressors across three discharge pressures. The IGSM45 curves (solid lines) consistently lie to the right of the V60 curves (dashed lines), indicating that at equivalent flow rates, IGSM45 consumes less power. This demonstrates a favourable performance-per-power ratio for IGSM45.

Fig. 10 (c) illustrates the variation of specific power with flow rate for both the IGSM45 (solid lines) and the V60 (dashed lines) across a range of discharge pressures. As expected, specific power decreases with increasing flow rate for all configurations, reflecting improved energy utilisation at higher flows. Notably, IGSM45 consistently exhibits lower specific power than V60 across the full range of flow rates and pressures, indicating more effective performance in terms of energy required per unit of delivered volume. The performance advantage of IGSM45 is particularly evident at low pressure ratio, where the gap is most pronounced. At higher pressures the difference narrows slightly.

Fig. 10 (d) presents the variation in volumetric efficiency with respect to the flow rate for both IGSM45 (solid lines) and V60 (dashed lines) across three discharge pressures. At lower discharge pressure (7 bar), IGSM45 consistently achieves higher volumetric efficiency,

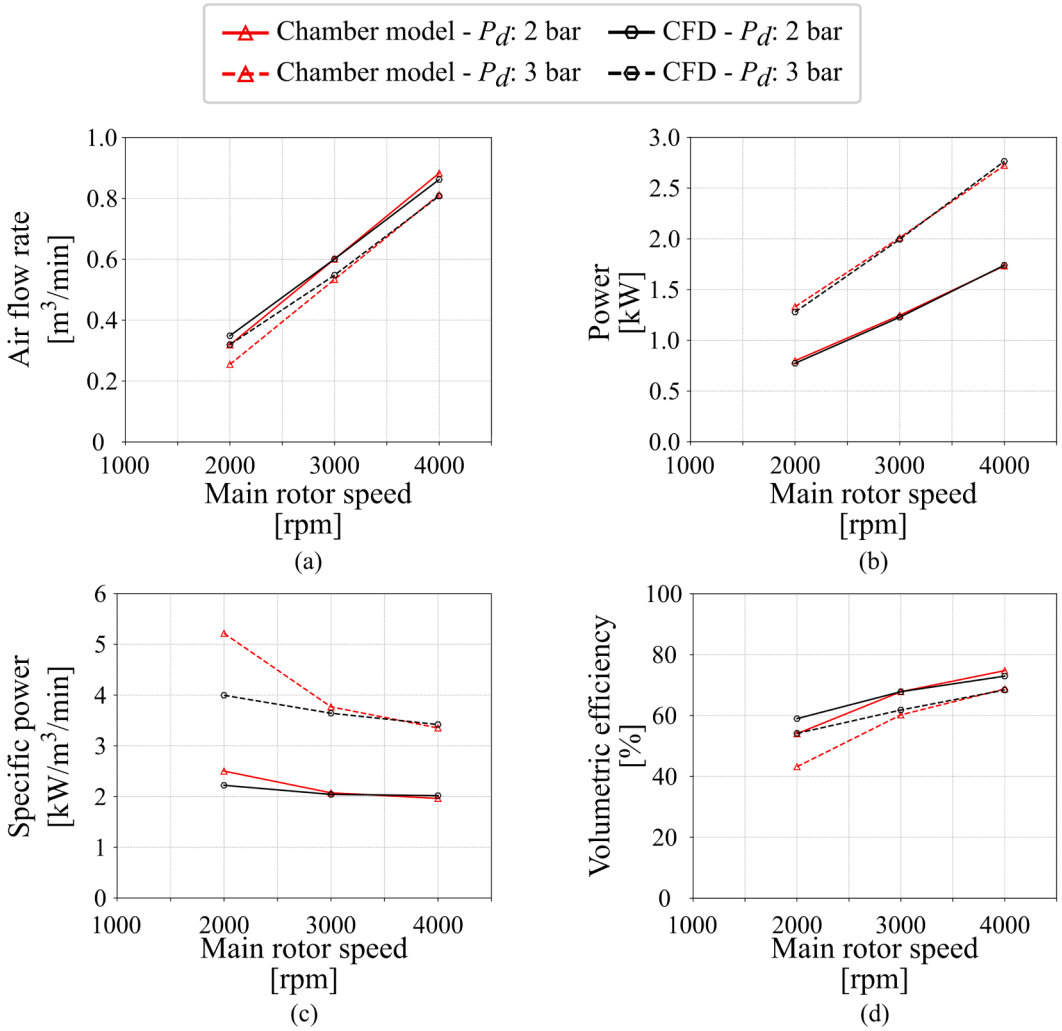

Fig. 8. Comparison between the chamber model and CFD results for the oil-injected internally geared screw machine configuration defined in Table 1, using operating conditions listed in Table 2. The subfigures present: (a) air flow rate, (b) indicated power, (c) specific power, and (d) volumetric efficiency across different main rotor speeds for two discharge pressures.

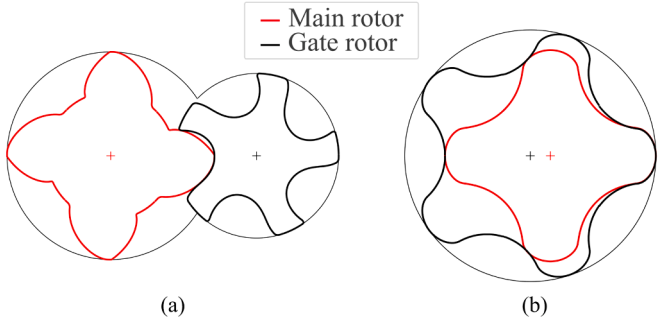

Fig. 9. Comparison of rotor profiles for the (a) conventional V60 twin screw compressor and (b) the internally geared screw machine IGSM45, shown in equivalent scale.

particularly at lower flow rates. However, at the highest discharge pressure of 13 bar, V60 slightly outperforms IGSM45. Nonetheless, both machines show improved efficiency with increasing flow rate.

Fig. 10 (e) illustrates the variation in adiabatic efficiency with respect to flow rate for both the IGSM45 (solid lines) and V60 (dashed lines) configurations across compared pressure ratios. The IGSM45 demonstrates consistently higher adiabatic efficiency over the full operating range compared to V60. As flow increases, both machines approach their peak adiabatic efficiencies, but IGSM45 maintains a more favourable adiabatic efficiency for all observed cases.

The comparison confirms that the internally geared screw machine, represented by IGSM45, consistently outperforms the conventional twin screw compressor (V60) at this scale. The results suggest that the internal gearing and compact design of IGSM45 enable superior thermodynamic performance, likely due to reduced leakage and lower heat transfer losses in small-scale configurations. This observation supports the long-standing hypothesis that IGSM technology is particularly well-suited for extending the lower size limit of screw compressors, potentially offering a competitive alternative to scroll compressors. Although IGSM shows clear advantages in the small-size range, its advantages are likely to become less significant as machine size increases, and this trend needs to be further investigated for larger machine configurations.

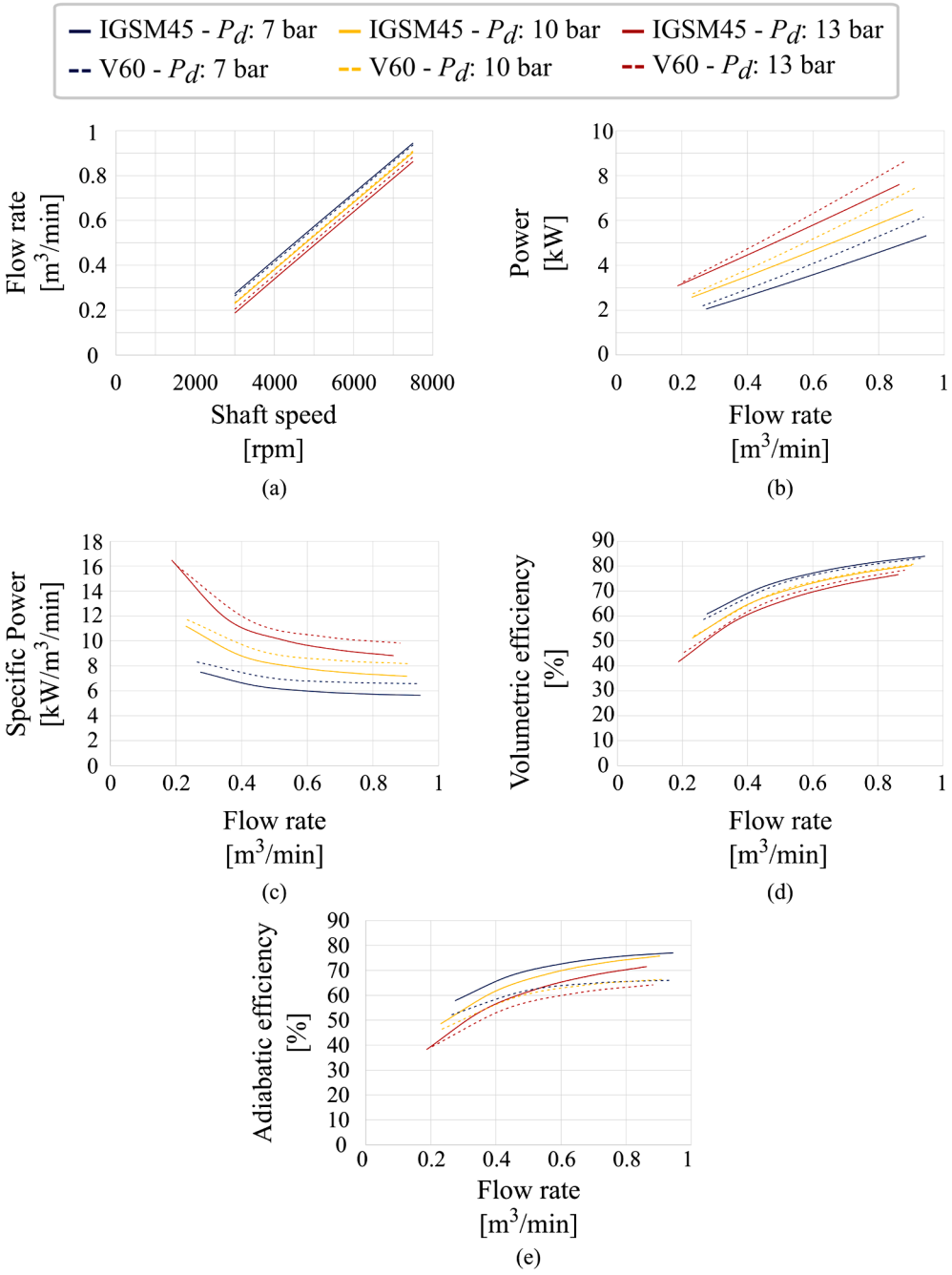

Fig. 10. Comparison of performance between the conventional V60 and the internally geared IGSM45 compressor across three discharge pressures. Results include variation of flow rate (a), indicated power (b), specific power (c), volumetric efficiency (d), and adiabatic efficiency (e).

5. Conclusions

Internally geared screw machines (IGSMs) remain a relatively novel type of compressor, with previous research primarily focusing on geometric modelling and preliminary performance assessments. Although several potential advantages over conventional twin screw compressors have been suggested, these have not yet been thoroughly investigated. This paper presents a comprehensive geometrical modelling framework for IGSMs, detailing all necessary procedures to analyse a wide range of machine configurations.

To evaluate the thermodynamic performance, an existing one-dimensional multi-chamber model was employed and verified against CFD results from prior studies. This verification confirms that the chamber model reliably captures the performance trends observed in higher-order models.

Using this verified framework, a comparative study was conducted between a conventional small-scale twin screw compressor and a geometrically equivalent IGSM design. This is the first such comparison performed using a chamber model, and the results clearly demonstrate the performance benefits of the IGSM configuration for small-scale applications. These findings support earlier hypotheses that IGSMs could effectively extend the lower size limit of screw compressors, offering a possible alternative to scroll compressors.

While the advantages of IGSMs are evident at smaller scales, it is possible that these benefits may reduce or reverse as machine size increases. Further research is therefore needed to investigate this behaviour across

a broader range of compressor sizes, both smaller and larger than those examined in this study.

CRediT authorship contribution statement

Halil Lacevic: Software, Methodology, Conceptualization; **Ahmed Kovacevic:** Validation, Supervision; **Sham Rane:** Investigation; **Matthew Read:** Supervision, Methodology.

Data availability

Data will be made available on request.

Declaration of competing interest

The authors declare that they have no known competing financial interests or personal relationships that could have appeared to influence the work reported in this paper.

Supplementary material

Supplementary material associated with this article can be found in the online version at 10.1016/j.rineng.2025.108793.

References

[1] K. Lu, I.A. Sultan, T.H. Phung, A literature review of the positive displacement compressor: current challenges and future opportunities, Energies 16 (20) (2023) 7035. https://doi.org/10.3390/en16207035

[2] N. Stosic, I. Smith, A. Kovacevic, Screw Compressors: Mathematical Modelling and Performance Calculation, Springer, Berlin, Berlin, 2005. https://doi.org/10.1007/b137216

[3] K. Hanjalic, N. Stosic, Development and optimization of screw machines with a simulation model-part II: thermodynamic performance simulation and design optimization, J. Fluids Eng. 119 (3) (1997) 664–670. https://doi.org/10.1115/1.2819296

[4] C. Wang, Z. Xing, W. Chen, Q. Yang, Z. He, Development of an oil free water-lubricated twin-screw air compressor, Appl. Therm. Eng. 143 (2018) 396–402. https://doi.org/10.1016/j.applthermaleng.2018.07.119

[5] S. Kennedy, M. Wilson, S. Rane, Combined numerical and analytical analysis of an oil-free twin screw compressor, IOP Conf. Series: Mater. Sci. Eng. 232 (2017) 012080. https://doi.org/10.1088/1757-899X/232/1/012080

[6] N. Basha, A. Kovacevic, S. Rane, Analysis of oil-injected twin-screw compressor with multiphase flow models, Designs 3 (4) (2019). https://doi.org/10.3390/designs3040054

[7] M. Rundo, Models for flow rate simulation in gear pumps: a review, Energies 10 (9) (2017) 1261.

[8] P.J. Gamez-Montero, E. Codina, R. Castilla, A review of gerotor technology in hydraulic machines, Energies 12 (12) (2019) 2423. https://doi.org/10.3390/en12122423

[9] M.G. Read, I.K. Smith, N. Stosic, Internally geared screw machines with ported end plates, IOP Conf. Series: Mater. Sci. Eng. 232 (2017) 012058. https://doi.org/10.1088/1757-899x/232/1/012058

[10] M.G. Read, I. Smith, N. Stosic, Influence of rotor geometry on tip leakage and port flow areas in gerotor-type twin screw compressors, Proc. Inst. Mech. Eng. Part E: J. Process Mech. Eng. 236 (1) (2020) 94–102. https://doi.org/10.1177/0954408920962412

[11] A. Kovacevic, N. Stosic, I.K. Smith, Screw Compressors: Three Dimensional Computational Fluid Dynamics and Solid Fluid Interaction, Springer, Berlin, Berlin, 2007.

[12] K. Vimalakanthan, M. Read, A. Kovacevic, Numerical modelling and experimental validation of twin-screw expanders, Energies 13 (18) (2020). https://doi.org/10.3390/en13184700

[13] Y. Li, X. Zhao, S. Liu, C. Wang, S. Shen, Y. Guo, Review and prospects of numerical simulation research on internal flow and performance optimization of twin-screw compressors, Energies 18 (10) (2025). https://doi.org/10.3390/en18102608

[14] H. Wu, H. Huang, B. Zhang, B. Xiong, K. Lin, CFD simulation and experimental study of working process of screw refrigeration compressor with R134a, Energies 12 (11) (2019). https://doi.org/10.3390/en12112054

[15] H. Lacevic, A. Kovacevic, N. Stosic, M. Read, On rotor profiling of internally geared screw machines, IOP Conf. Series: Materi. Sci. Eng. 1322 (2024) 012006. https://doi.org/10.1088/1757-899X/1322/1/012006

[16] M.G. Read, N. Stosic, I.K. Smith, The influence of rotor geometry on power transfer between rotors in gerotor-type screw compressors, ASME J. Mech. Design 142 (7) (2020) 073501. https://doi.org/10.1115/1.4045508

[17] M. Read, N. Stosic, I. Smith, Performance analysis of internally geared positive displacement machines, in: Proceedings of the 24th International Compressor Engineering Conference, 2532, Purdue University, 2018.

[18] S. Rane, A. Kovačević, M. Read, Development of numerical grid and CFD model for analysis of oil-Injected IGSM, in: M. Read, S. Rane, I. Ivkovic-Kihic, A. Kovacevic (Eds.), 13th International Conference on Compressors and Their Systems (ICCS 2023), Springer Proceedings in Energy, Springer, Cham, 2024. https://doi.org/10.1007/978-3-031-42663-6_41

[19] J. Colbourne, The geometry of trochoid envelopes and their application in rotary pumps, Mech. Mach. Theory 9 (3–4) (1974) 421–435. https://doi.org/10.1016/0094-114x(74)90025-1

[20] D. Vecchiato, A. Demenego, J. Argyris, F.L. Litvin, Geometry of a cycloidal pump, Comput. Methods Appl. Mech. Eng. 190 (18–19) (2001) 2309–2330. https://doi.org/10.1016/s0045-7825(00)00236-x

[21] F.L. Litvin, A. Fuentes, Gear Geometry and Applied Theory, Cambridge University Press, Cambridge, 2nd edition, Cambridge, 2004.

[22] A. De Martin, G. Jacazio, M. Sorli, Optimization of gerotor pumps with asymmetric profiles through an evolutionary strategy algorithm, Machines 7 (1) (2019) 17. https://doi.org/10.3390/machines7010017

[23] A. Robison, Design of Gerotor Gear Geometry by Multi-Objective Optimization, Ph.d. thesis, Purdue University, 2021.

[24] D. Genta, G. Ghigo, M. Milanese, A. Pennacchi, Influence of rotor profile geometry on the performance of an original low-pressure gerotor pump, Mech. Mach. Theory 105 (2016) 245–261. https://doi.org/10.1016/j.mechmachtheory.2016.02.012

[25] M. Read, Epitrochoidal gerotor profiles with asymmetric lobes, in: Proceedings of the 26th International Compressor Engineering Conference, West Lafayette, Indiana, 2022.

[26] S. Rane, A. Kovačević, N. Stošić, Grid generation for CFD analysis and design of a variety of twin screw machines, Designs 3 (2) (2019). https://doi.org/10.3390/designs3020030

[27] N. Basha, A. Kovacevic, S. Rane, Numerical investigation of oil injection in screw compressors, Appl. Therm. Eng. 193 (2021) 116959. https://doi.org/10.1016/j.applthermaleng.2021.116959

[28] A. Aydın, T. Engin, A. Kovacevic, Design optimisation of a screw compressor with a focus on rotor depth: a computational fluid dynamics approach, Int. J. Refrig 170 (2025) 385–397. https://doi.org/10.1016/j.ijrefrig.2024.12.001

[29] S. Yang, H. Ouyang, Y. Wu, L. Wang, L. Mei, H. Wang, CFD simulation for the internal pressure characteristics of an oil-injected twin-screw refrigeration compressor, Int. J. Refrig 126 (2021) 143–154. https://doi.org/10.1016/j.ijrefrig.2021.01.020

[30] S. Rane, A. Kovačević, N. Stosic, Analysis of a R1234ze(E) twin screw compressor using thermodynamic chamber and 3D CFD models, in: 14th International Conference on Compressors and Their Systems (ICCS 2025), Springer Proceedings in Energy, Springer, 2025.

[31] VMC Italy, V60 Oil Inject Screw Compressor - Technical Catalogue, VMC Italy, Italy,